6 Soft-matter Project

Project Leader: Hideki Seto

6-1 Introduction

Soft matter is a subfield of condensed matter comprising a variety of physical states that are easily deformed by thermal stresses or thermal fluctuations. They include liquids, colloids, polymers, liquid crystals, amphiphilic molecules, and a number of biological materials. These materials often self-organize into mesoscopic structures that are much larger than the microscopic scale (the arrangement of atoms and molecules), and yet are much smaller than the macroscopic scale of the material. The properties and interactions of these mesoscopic structures may determine the macroscopic behavior of the material. In spite of the various forms of these materials, many of their properties have common physicochemical origins, such as a large number of internal degrees of freedom, weak interactions between structural elements, and a delicate balance between entropic and enthalpic contributions to the free energy. These properties lead to large thermal fluctuations, a wide variety of forms, sensitivity of equilibrium structures to external conditions, macroscopic softness, and metastable states.

With this background, we are investigating the structural properties of soft matter such as liquids and amphiphilic molecules.

6-2 Kinetic process of the formation and reconstruction of small unilamellar vesicles

Biomembranes comprise a mixture of amphiphiles: phospholipids, cholesterol, membrane proteins, etc. In other words, a biomembrane is a kind of amphiphile mixture system. According to studies on surfactant mixtures, not only the molecular shape but also the phase separation of amphiphiles play a key role in the structural formation of a multicomponent system. In this study, we are focusing on the phospholipid mixture of dimyristoylphosphatidylcholine (DMPC; 14 carbons/chain) and dihexanoylphosphatidylcholine (DHPC; 6 carbons/chain), which show various kinds of self-assemblies depending on the composition and temperature: globular, discoidal, ribbon-like micelles, punctuated lamellae, etc. The planes and rims of these structures are mainly composed of DMPC and DHPC, respectively, and the phase separation between the lipids governs the structural formation. Under certain conditions, small unilamellar vesicles (SUVs; 10–100 nm in radius) are spontaneously formed from bilayered micelles (bicelles; approximately 10 nm in radius) at a temperature jump from below the chain melting temperature of DMPC, T_c (23°C), to above the T_c. Interestingly, nanopores are formed on the SUV surface when the temperature approaches T_c. Since the degree of phase separation generally depends on temperature, this result suggests that a decrease in temperature induces phase separation between lipids and the rim consisting of DHPC molecules stabilizes the nanopores.

In order to understand the effect of temperature on the SUV structure and nanopore formation, we performed conventional small-angle neutron scattering (SANS) experiments after temperature jumps from 0°C to 50°C (path A) and from 50°C to 30, 27, or 25°C (paths B, C, and D, respectively). Figure 1 shows the obtained SANS profiles depending on the temperature path, in which the period of fringes is inversely proportional to the size of SUVs. Whereas the SANS profile after the temperature jump from 50°C to 30°C (path B) is almost the same as that before the temperature jump (path A), those to 27 and 25°C (paths C and D, respectively) drastically changed. Since the period of fringes becomes shorter, this indicates an increase in the size of SUVs. To the best of our knowledge, such structural change has not been reported for any amphiphile mixture systems.

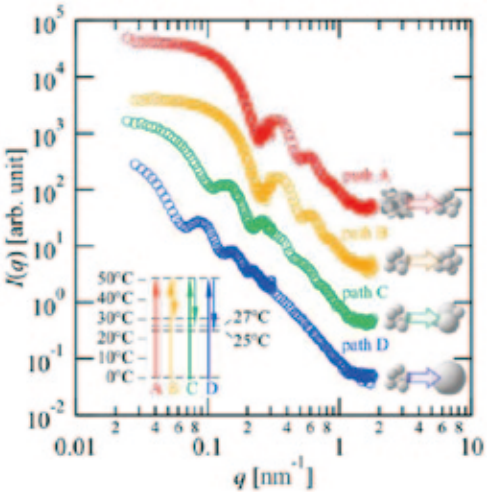

Fig. 1: SANS profiles after temperature jumps from 0°C to 50°C (path A) and from 50°C to 30, 27, or 25°C (path B, C, and D).

Next, we investigated the kinetic process of the structural change of SUVs using the time-resolved SANS (TR-SANS) technique. Figure 2(a) shows the results of the TR-SANS experiment after the temperature jump from 50°C to 25°C (path D). First, SUV fringes immediately disappeared after the temperature jump, and a profile with a shoulder was observed instead. This profile is inconsistent with that of SUVs, but consistent with that of bicelles whose surface area is identical with that of the SUVs before the temperature jump. Therefore, the change in the profiles indicates the transformation of SUVs into bicelles. After the transformation, the shoulder of bicelles gradually shifted to lower q over time and the SUV fringes gradually appeared. Since the q-value of the shoulder is inversely proportional to the radius of bicelles, this indicates that the bicelles grow with time and transform into SUVs at a certain size. Hereafter, this structural change is called “SUV reconstruction”.

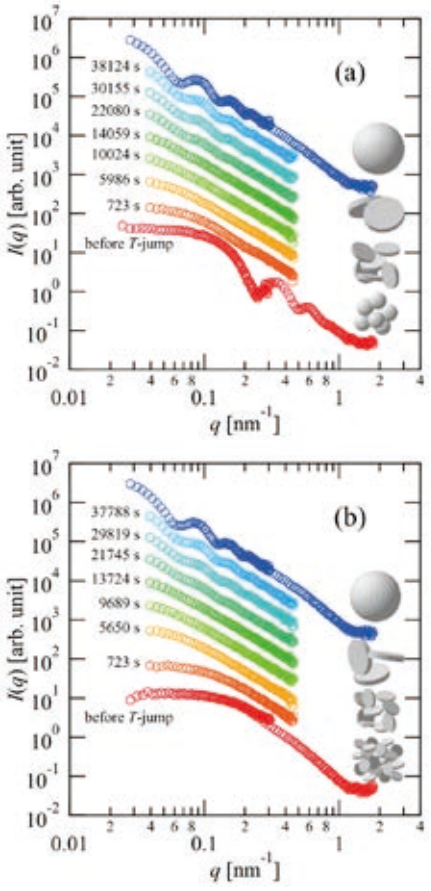

Fig. 2: Results of TR-SANS experiments after the temperature jump (a) from 50°C to 25°C and (b) from 0°C to 25°C.

For comparison, the kinetic process after the temperature jump from 0°C to 25°C was also investigated, in which the initial structure is not a SUV but a bicelle. In this case, the shoulder of bicelles gradually shifted to lower q over time and the SUV fringes gradually appeared as shown in Fig. 2(b). That is, the only difference between these two processes is the transformation process from SUVs to bicelles immediately after the temperature jump, which could be the key process for the SUV reconstruction.

For quantitative discussion, we evaluated the temperature dependence of the line tension from a simple relation with the SUV radius after the transition from bicelles R^* and bending modulus κ. Table 1 shows the temperature dependence of R^* and γ (κ is taken from the literature): γ decreases as R^* increases for temperatures approaching T_c. The decrease in γ indicates that the phase separation between lipids was enhanced and that a DHPC-rich domain stabilized the rims of bicelles.

Table 1 Temperature dependence of the thermodynamic parameters.

T(°C)	R^*(nm)	κ (k_BT)	γ (k_BT/nm)
50	12.07	28	9.3
30	20.44	31	6.1
27	28.64	37	5.2
25	48.0	19	1.6

Finally, the sequence of the SUV reconstruction process is summarized in Fig. 3. Figure 3 (a) shows the free energy densities depending on the vesicle size at 25°C. Immediately after the temperature jump from 0°C, bicelles (aperture angle of a cup-shaped membrane $\theta = 180°$) are more stable than SUVs ($\theta = 0°$) as can be seen from the top profile in the figure. The bicelle edges are, however, not very stable because the phase separation between lipids is not strong above T_c, and they fuse to each other in order to reduce the rim area. After the bicelle growth, the local minimum at $\theta = 180°$ disappears at the critical size as can be seen from the bottom profile, and the bicelles transform into SUVs. In the case of the temperature jump from 50°C, the potential minimum at $\theta = 0°$ is very shallow as in the middle profile, and the perforation caused by the phase separation makes SUVs transform into bicelles. After the transformation, bicelles revert to SUVs after the bicelle growth as the temperature jumps from 0°C. In contrast, the potential minimum at $\theta = 0°$ after the temperature jump from

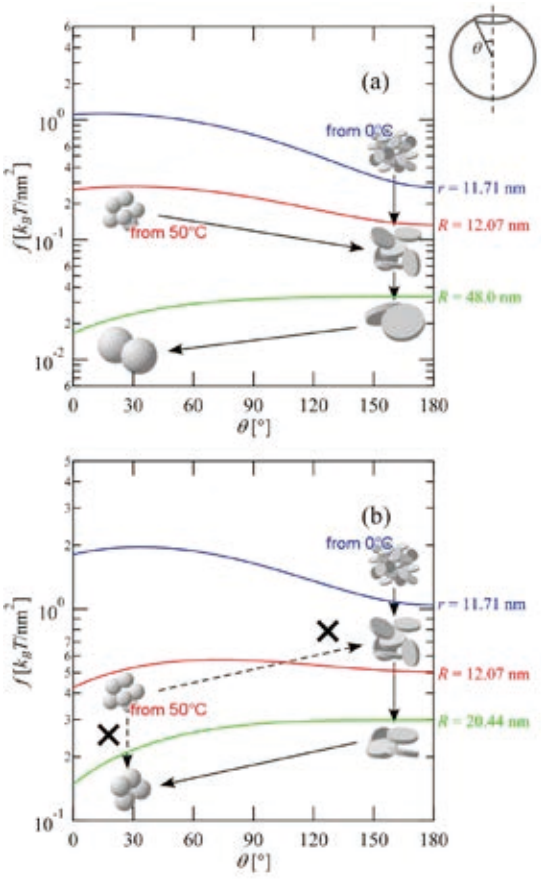

Fig. 3: Free energy densities depending on the vesicle size at (a) 25°C and (b) 30°C. The top and middle profiles indicate the free energy densities immediately after the temperature jump from 0°C and 50°C, respectively. The bottom profile represents the transformation from bicelles to SUVs at the critical size.

50°C to 30°C is very deep, as shown by the middle profile in Fig. 3(b). This indicates that the phase separation can induce perforation but cannot induce transformation into bicelles. Hence, SUVs are kinetically trapped after the temperature jump from 50°C to 30°C.

References
N. L. Yamada, et al., Phys. Rev. E **79** (2009) 032902.
N. L. Yamada, Langmuir **28** (2012) 17381.

6-3 The effect of an antagonistic salt on a mixture of D_2O and 3MP

It has been known that the phase behaviors of binary mixtures of water and organic solvent change upon adding salt. In most cases, both cations and anions of salts are hydrophilic and attract water molecules, and the solubility of water and organic solvent decreases with salt concentration and the 2-phase region is enhanced. Various experiments have been performed to verify the existence of solvation clusters to explain the phase behavior, and showed that the diameters of clusters are on the order of several tens of angstroms.

Recently, we showed the opposite phase behavior in a binary mixture composed of deuterated water (D_2O) and 3-methylpyridine (3MP) upon adding the antagonistic salt, sodium tetraphenylborate ($NaBPh_4$). $NaBPh_4$ is composed of hydrophilic cations and hydrophobic anions, which are distributed heterogeneously in the mixture because cations and anions either attract water or 3MP molecules. This phase behavior was explained as follows: the solvation clusters of D_2O and 3MP should interact electrostatically and $NaBPh_4$ molecules behave as surfactants. In addition, the authors discovered a nanometer-scale periodic structure in the 1-phase region. When the concentration of salt was less than 60 mmol/L, a broad single peak profile was observed by small-angle neutron scattering (SANS). When the salt concentration was increased above 60 mmol/L up to 250 mmol/L in water-rich mixtures, the SANS profiles drastically changed to multi-peak profiles.

In this study, we tried to confirm the effect of the preferential solvation on the mixture of D_2O and 3MP with a different kind of antagonistic salt, tetraphenylphosphonium chloride (PPh_4Cl) (which we call an "inversely antagonistic" salt), composed of hydrophobic cations and hydrophilic anions. The phase behavior was observed by visual inspection (see Fig. 4). In a binary mixture of D_2O and 3MP, cloud points were observed between 37°C and 67°C depending on φ_{3MP}. By adding 5 mmol/L of PPh_4Cl to the binary mixture, the cloud points are raised and the 2-phase region shrinks. As we increase C_{salt}, the 2-phase region shrinks more and disappears above C_{salt} = 20 mmol/L. This behavior is similar to our previous observation in the mixture of D_2O, 3MP and $NaBPh_4$. This evidence indicates that the preferential solvation of cations and anions of an antagonistic salt increases the solubility of D_2O and 3MP independent of the kind of antagonistic salt.

The nano-scale structure was observed by SANS measurement using the NG7-30 m SANS instrument at the National Institute of Standards and Technology (NIST) Center for Neutron Research. Scattering intensities of the samples of C_{salt} = 85 mmol/L measured by SANS are depicted in Fig. 5. For better visualization, the profiles at higher temperatures are

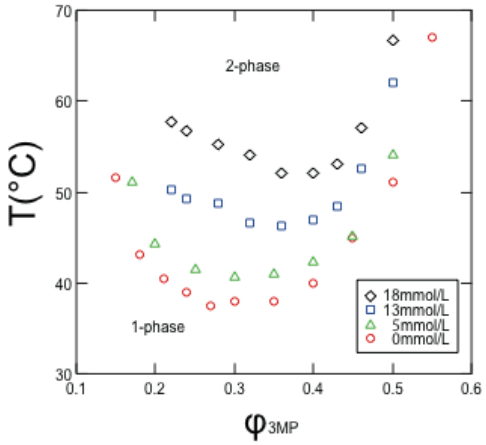

Fig. 4: Phase diagram obtained by visual inspection. Open circles indicate cloud points of the binary mixture of D_2O and 3MP. Open triangles, squares, and diamonds correspond to those of ternary mixtures with C_{salt} = 5 mmol/L, 13 mmol/L, and 18 mmol/L, respectively. Errors are hidden within the size of plot characters.

shifted by multiplying by 2.5 for T = 31°C, 5 for T = 54°C, and 10 for T = 73°C. At this salt concentration, the 2-phase region shown in Fig. 4 has already disappeared. However, in all the volume fractions of 3MP, the scattering intensities increase with increasing temperature. This result indicates that the concentration fluctuation exists in the 1-phase region and increases with increasing temperature. The absolute intensities from the sample with φ_{3MP} = 0.35 are about 10 times larger than those from the other samples, which means that the sample with φ_{3MP} = 0.35 is closer to the critical concentration.

As shown by the dashed lines in Fig. 5, the SANS profiles are fitted with Ornstein-Zernike's formula:

$$I_{OZ}(Q) = \frac{I_0}{1+\xi^2 Q^2}, \qquad (1)$$

where I_0 is proportional to the osmotic compressibility, and ξ is the correlation length. The profiles from the samples with φ_{3MP} = 0.35 and 0.54 are explained well by Eq. (1). On the other hand, the results fitted to Eq. (1) of the SANS profiles from the sample with φ_{3MP} = 0.09 are not very close as shown by the dashed line for the profile at T = 73°C. The small shoulder observed around Q = 0.1 Å^{-1} suggests that a periodic structure coexists with the concentration fluctuation. Following the previous results from ternary mixtures with $NaBPh_4$, we apply the formula given by Onuki and Kitamura:

$$I_{OK} = \frac{I_{OK0}}{1+[1-\gamma_p^2/(1+\lambda_D^2 Q^2)]\xi^2 Q^2}, \qquad (2)$$

where non-dimensional parameter γ_p indicates the degree of solvation asymmetry between cations and anions which is related to Gibbs free energy transfer, and λ_D is the Debye screening length which is set to λ_D = 10.4 Å. In the case of an antagonistic salt, γ_p >1 and the peak position corresponding to the repeat distance of the CDW structure is calculated as

$$Q_m = \frac{\sqrt{\gamma_p - 1}}{\lambda_D}. \qquad (3)$$

As shown by the solid lines in Fig. 5, Eq. (2) explains well the SANS profiles from the sample with φ_{3MP} = 0.09. The calculated Q_ms' are about 0.06 Å^{-1} for all the temperatures observed. The evidence that the

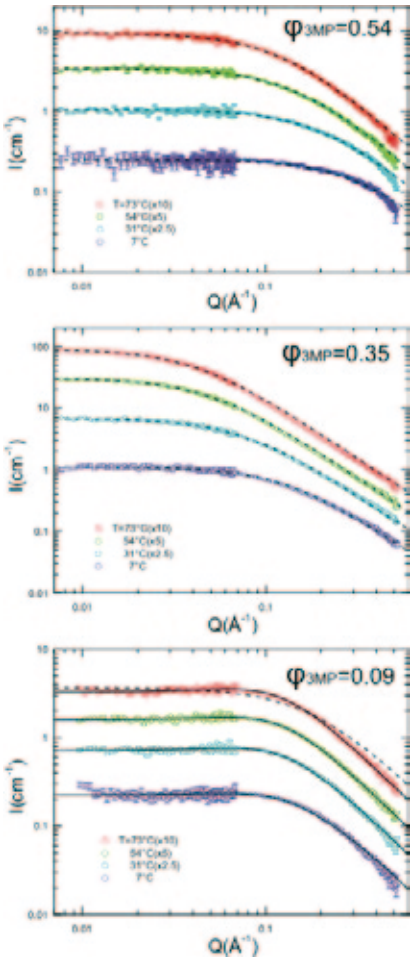

Fig. 5: Temperature dependence of the SANS profiles for the samples with φ_{3MP} = 0.54 (upper), 0.35 (middle), and 0.09 (lower). The salt concentration was fixed at 85 mmol/L. For better visualization, the data at higher temperature are shifted by a multiplication factor of 2.5 for T = 31°C, 5 for T = 54°C, and 10 for T = 73°C, respectively. Error bars represent ±1 standard deviation.

SANS profiles are explained by Eq. (2) suggests that the CDW structure is also induced in the water-rich mixture of D_2O and 3MP by adding "inversely antagonistic" salts. Furthermore, the concentration fluctuation increases with increasing temperature as is the case with "normally antagonistic" salts. However, the characteristic repeat distance of the CDW structure does not change with temperature unlike "normally antagonistic" salts.

The present results indicate that the solvation effect of "inversely antagonistic" salts on a mixture of D_2O and 3MP is similar to that of "normally antagonistic" salts. The electrostatic force between a cluster of 3MP molecules attracted by hydrophobic cations and a cluster of D_2O molecules attracted by hydrophilic anions decreases the interfacial tension between the solvents. From the experimental evidence, we generalize that the surface activities of antagonistic salts have the same tendency as those of surfactants.

The ability to form a long-range periodic structure could also be general for these kinds of salts. However, the regularity of the structure might depend on the kinds of salt and interaction with solvent molecules. In the case of $NaBPh_4$ at $\varphi_{3MP} = 0.09$, a typical value of the degree of solvation asymmetry γ_p is around 2, which is two times larger than that for PPh_4Cl. In the present case, the heterogeneous distribution of ions may not be distinct and the micro phase separation of D_2O and 3MP is weak. Thus the composition range of the structure in the ternary mixture with PPh_4Cl is narrower than that with $NaBPh_4$.

There are two possibilities why the lamellar phase in the present mixture is not observed. One is that the observed conditions did not cover the range of the lamellar phase. The other possibility is that the lamellar phase is intrinsically absent in the mixture with PPh_4Cl. As we described in the previous paper, the lamellar structure is stabilized by the balance between the entropic effect of ions and the electrostatic double-layer repulsion. This balance is easily disturbed by the size difference of ions and solubilities of ions into solvents. Thus it is possible that the delicate balance required to stabilize the lamellar structure is broken in the present mixture.

References

K. Sadakane et al., Chem. Lett. **41** (2012) 1075.